IL NUOVO CIMENTO Vol. 37 C, N. 4 Luglio-Agosto 2014
DOI 10.1393/ncc/i2014-11800-9

Communications: SIF Congress 2013

Muon tomography effectiveness in detecting orphan sources in scrap metal

A. Rigoni Garola(*)

Dipartimento di Fisica e Astronomia, Università di Padova - Padova, Italy
INFN, Sezione di Padova - Padova, Italy

ricevuto l'1 Febbraio 2014; approvato il 3 Aprile 2014

Summary. — The detection of sealed orphan sources inside scrap metal transportation is a crucial concern for the steel industry, because an accidental melting of radioactive material can produce severe environmental harm. The technique of muon tomography appears to be suitable for this purpose, because it allows to discriminate high-Z materials, measuring multiple scattering of cosmic ray muons crossing the cargo. A European project (RFSR-CT-2010-000033) to exploit this technique started in 2010 and finished in 2012. The aim of the project was to design an inspection portal able to detect lead-shielded radioactive sources hidden in scrap metal containers using cosmic rays. The reconstruction algorithms and their performances were studied in a full simulated environment.

PACS 42.30.Wb – Image reconstruction; tomography.
PACS 89.60.Ec – Environmental safety.
PACS 89.20.Bb – Industrial and technological research and development.

1. – Introduction

The potential presence of radioactive material in scrap metal represents a well known issue for the use of recycled metals in manufacturing. In the present time the scrap is an important source for the steel production, contributing to a large fraction (about 50%) of the final product. The scrap reuse through melting offers substantial savings in terms of raw materials and energy, making the recycling of scrap worthwhile for both the environment and steel industries. On the other hand, radioactive sources, that are commonly used in medicine, industry and research, can become associated with scrap metal in various ways and, if not discovered, they can be incorporated into steel, slags or powders through the melting process. Radioactive sources hidden inside scrap metal containers mainly depends on either *naturally occurring radioactive material* (NORM) or *orphan*

(*) E-mail: andrea.rigoni@pd.infn.it

sources (OS). IAEA([1]) defines OS as radioactive sources which are not under regulatory control, either because they have never been or because they have been abandoned, lost, misplaced, stolen or otherwise transferred without proper authorization. NORM sources generally do not pose risks of real contamination, but they are able to trigger false alarms to the control sensory in melting facilities. On the contrary, OS represent a concrete risk of serious environmental detriment and possible harm for the population, but they are usually well sealed and not always automatically detected by their emissions.

Increasing international attention has been given to the control of radioactive sources, for example, through the IAEA *"Code of Conduct on the Safety and Security of Radioactive Sources"*. However, there does not appear to have been any relevant reduction in the number of reported cases. In recent years, numerous accidents have occurred contaminating all the production line and involving, in some cases, the discovery of radioactive substances in the steel output from the melting process. These accidents have proved to be very costly in terms of the recovery and cleanup operations required, and also of the potential loss of confidence of the industry in scrap metal as a resource. Those motivations have led the steel industry to seek for a solution to this problem. The site of intervention seems to be the transportation entrance, before any scrap reprocess occurs; therefore a portal to inspect the entire truck appears to be the best option.

Cosmic Muon Tomography (CMT) is a non-invasive imaging technique, recently proposed [1] by a research group of LANL([2]), that is able to produce images of the density distribution of an enclosed volume using the natural cosmic ray radiation. This radiation at sea levels is largely composed of high-penetrating muons that hit the ground with a rate of $\approx 170\,\mathrm{Hz/m^2}$. Measuring the interaction of muons traversing the truck and the cargo material, CMT is able to effectively discriminate high-Z materials from scrap, giving a map of material density distribution, and providing a chance to find out possible hidden OS through their dense shields. Taking advantage of the positive results of this technique applied to the first large volume prototype of muon tomography [2], European Community funded Mu-Steel project [3] (July 2010, Dicember 2012). The aim was to design an inspection portal able to detect shielded radioactive sources hidden in scrap metal containers, using cosmic rays.

The following section contains a brief description of the principles of CMT. In sect. **3** the design of Mu-Steel portal for inspection of truck containers is described. Sections **4** and **5** present the analysis procedure and the results obtained for simulated cargoes.

2. – Muon tomography

Muons are charged heavy particles and their interaction with matter is a composition of many small angle deflections, mainly due to Coulomb scattering from nuclei. The average angular difference between the particle direction entering and exiting a given homogeneous volume depends on the thickness as well as on the nature of the material. In particular it depends on a physical quantity X_0 called radiation length, which is function of the examined material density and of its atomic and mass numbers.

To obtain the tomographic image, the Multiple Coulomb Scattering (MCS) model [4] is used. For each muon we can define two independent planes containing the muon

([1]) International Atomic Energy Agency, the world's center of cooperation in the nuclear field within the United Nations family from 1957.
([2]) Los Alamos National Laboratories.

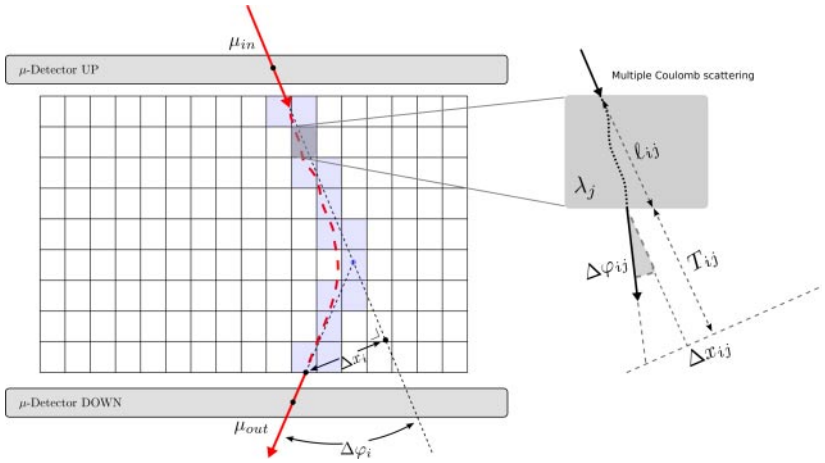

Fig. 1. – A schematic representation of the scattering of a single muon through the voxelized volume (sketch on the left). The quantities $\Delta\varphi_i$ and Δx_i are the data measured form detectors. The hidden variables modeled by the MCS event in one voxel are also detailed (sketch on the right) and are the input of the likelihood function for the tomographic reconstruction. See sect. **2** for details.

incident direction for which the distribution of projected deflection is roughly Gaussian with zero mean. For high-energy muons and low thickness the variance can be approximated as:

$$\sigma^2_{\Delta\varphi} = \ell \cdot \frac{b^2}{p^2}\lambda, \qquad \text{where} \qquad b \simeq \frac{15\,\text{MeV}}{c} \tag{1}$$

and p is the particle momentum. The quantity $\lambda = 1/X_0$ is defined as the Linear Scattering Density (LSD) and represents the mean square scattering angle per unit of length in the traversed material. In table I the λ-values are reported for some selected materials.

The goal of the tomographic reconstruction is to obtain a three-dimensional distribution of the scattering density of the material contained in the inspected volume. Therefore, as sketched in fig. 1, the detectors setup is designed to measure the entering and exiting directions of muons that traverse the reconstructing volume. The figure sketches a particular case in which both the incoming and the outgoing muon directions belong to

TABLE I. – *Linear scattering density values of some elements, evaluated from radiation length reported in* [5].

	Al	Fe	Cu	W	Pb	U
Atomic number	13	26	29	74	82	92
Mass density (g/cm^3)	2.7	7.9	8.9	19.3	11.3	19.0
LSD (rad^2/cm)	0.11	0.57	0.70	2.9	1.8	3.1

a plane perpendicular to the detectors. The experimental data are the measured scattering angle and displacement. They are the quantities $\Delta\varphi_i$ and Δx_i that are illustrated on the left of the figure where a schematic representation of the scattering process of the i-th muon is shown. In our formalism the displacement is defined as the projected distance between the incoming muon trajectory and the point where the outgoing trajectory exits the inspected volume. The distribution of scattering angle and displacement may be characterized as jointly Gaussian [4], with zero mean and

$$\sigma_{\Delta x} = \frac{\ell^2}{3}\sigma_{\Delta\varphi}. \tag{2}$$

The space of analysis is further divided into finite volume elements called voxels; each of them is assumed to have uniform scattering density. The technique relies on estimating the linear scattering density set λ through the maximization of a proper likelihood function. The effects of a muon multiple scattering inside the single j-th voxel are zoomed-in on the right of fig. 1. This sketch shows how the values of scattering angle and displacement can be thought as a composition of the MCS quantities in each voxel of defined density. Thereupon a multivariate variable can be associated to each muon and voxel, representing the j-th component of the acquired data due to the λ_j density. This variable is called hidden because it is not directly measurable and it is expressed as

$$H_{ij} = \begin{bmatrix} 1 & 0 \\ T_{ij} & 1 \end{bmatrix} \begin{bmatrix} \Delta\varphi_{ij} \\ \Delta x_{ij} \end{bmatrix}, \tag{3}$$

where the matrix containing T_{ij} represents the projection on the plane where the total displacement effect is measured. The distribution of H_{ij} is also Gaussian (always in the small angle approx.) with zero mean and covariance matrix given by

$$\Sigma_{H_{ij}} = W_{ij}\frac{\lambda_j}{p_i^2}, \quad \text{where} \quad W_{ij} = \begin{pmatrix} \ell_{ij} & \ell_{ij}\,T_{ij} + \frac{{\ell_{ij}}^2}{2} \\ \ell_{ij}\,T_{ij} + \frac{{\ell_{ij}}^2}{2} & \ell_{ij}\,{T_{ij}}^2 + {\ell_{ij}}^2\,T_{ij} + \frac{{\ell_{ij}}^3}{3} \end{pmatrix}. \tag{4}$$

The measured data is finally the sum of the defined hidden variables along the muon trajectory path,

$$D_i = \sum_j H_{ij} + \epsilon_i \quad \rightarrow \quad \Sigma_{D_i} = \sum_j W_{ij}\frac{\lambda_j}{p_i^2} + E_i, \tag{5}$$

where the terms ϵ_i and E_i represent the measurement errors and their covariance, respectively.

To find the best fit of λ-values, we used an iterative statistical approach proposed in [6] called the Expectation Maximization algorithm [7]. Rather than directly computing the maximum likelihood of the data, the method expresses the expected likelihood of all the hidden variables conditioned, in each iteration, by the measures and the λ value. Thus

an iterative formula is proved to converge to the maximum of the measurement likelihood using the following auxiliary function:

$$
\begin{aligned}
Q_{\mathrm{DLR}}(\lambda|\lambda^{(n)}) &= \mathbb{E}_{H|D,\lambda^{(n)}}\left[[\log \Pr(H, D|\lambda)]\right] \\
&= \sum_{i,j}\left(-\frac{r}{2}\log\lambda_j - \frac{1}{2}\mathbb{E}_{H|D,\lambda^{(n)}}\left[H_{ij}^T \Sigma_{H_{ij}}^{-1} H_{ij}\right]\right) + \text{const.},
\end{aligned} \tag{6}
$$

where in r we set the dimension of the multivariate H_{ij}, and in the const. argument we grouped together all the terms not concerning the density. For every voxel, the maximum is analytically computed by setting the first derivative of Q to zero. The solution provides an iterative density update:

$$
\frac{\partial Q_j}{\partial \lambda_j} = 0 \qquad \rightarrow \qquad \lambda_j^{(n+1)} = \lambda_j^{(n)} + \left\langle s_{ij}^{(n)} \right\rangle . \tag{7}
$$

The value of the update is the average of s_{ij}, expressed by

$$
s_{ij}^{(n)} = \frac{{\lambda_j^{(n)}}^2}{r p_i^2}\left[\mathrm{Tr}(\Sigma_{D_i}^{-1} W_{ij} \Sigma_{D_i}^{-1} D D^T) - \mathrm{Tr}(W_{ij}\Sigma_{D_i}^{-1})\right], \tag{8}
$$

that represents the expected value of the quadric form in (6) conditioned to the measured data and the state of λ at current iteration.

3. – Muon portal design

The goal of the Mu-Steel project was to detect a small source shield inside a truck container volume filled with scrap metal in short average acquisition times (about 5 minutes). The time constraint was required to allow the scan to be performed with a minimal impact on the queuing schedules of the steel mill facility hosting the portal. The full scale portal for the Mu-Steel project has been completely simulated. It was designed with dimensions $18 \times 5 \times 6$ meters to fit a 40 ft container, although simulations presented here have been performed with the most commonly used 20 ft model. The portal sensitive system is composed of four muon detectors chambers: an upper and a lower detector, and two lateral detectors to increment data acquisition rate with high azimuthal angle muons. The muon detector has been designed as an assembly of orthogonal units, called superlayers. This design modularity was foreseen to ease the construction, installation and maintenance operations of a real operative portal. A schematic of the portal is shown in fig. 2 The truck support was composed by an array of timber wood beams to minimize the multiple scattering of the muons outside the volume of interest. All the materials simulation and particle physics were done with GEANT4 package [8]. A truck minimalistic model filled by simulated scrap was placed inside the portal. Metal scrap has been generated as a collection of small volumes whose density spans from air to iron. The density distribution average was set to 10% of iron. It corresponds to the measured average density of a real container filled with finegrained scrap metal.

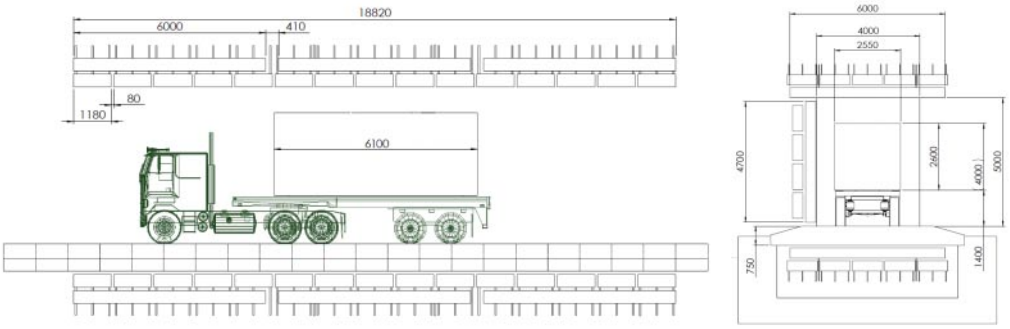

(a) (b)

Fig. 2. – A schematic view of the portal design.

4. – Image reconstruction procedure

The image reconstruction starts from the muon path tracing. The portal detectors are composed of many muon drift tubes of circular section with a wire anode at the center. Each tube measures the distance of muon passage from the anode wire. The collection of these distances in each detector is then fitted to a straight line, building the most probable track for both the entering and the exiting of the muon trajectory trough the experiment.

The analyzed volume lies among the detector chambers and, as shown before, it has to be properly voxelized to form a tree-dimensional image. The size of voxels must be optimized in relation to a sufficient muon statistic collected inside of them, and to the correct resolution needed for the target. Our tests have been performed using 5 cm and 7 cm sided cubic voxels, in order to investigate 2 liter and 5 liter source shields. The voxel grid was set to be uniform spaced; for these sizes the image counts 604800 and 223600 voxels respectively. From the fitted trajectory of the particle, the system raytraces the most probable path inside the voxels volume. The real path followed by the muon is guided by multiple scattering events inside the volume. Only the input and output tracks are known and they do not generally intersect each other. To approximate the muon path trajectory inside the container we used the Point of Closest Approach (PoCA), *i.e.* the point that minimize both the distances between the two fitted directions. A specific fast raytracing algorithm provides all the lengths of the intersections of the path with the voxels volume.

The portal setup has been simulated, and the muon datasets have been generated through the GEANT4 Monte Carlo toolkit. We used data acquired in time intervals from 2 to 6 minutes, *i.e.* from 480000 to 1450000 muons. A reconstructed image of a simulated container filled with scrap metal hiding a 5 liter source shield is shown in fig. 3a. In the reconstruction setup presented we simulated the truck battery, the gearbox and the differential housing using a solid block of high-density material as a reference. For the acquisition times fixed by the project, the large dataset still gives a low statistic of muons crossing finegrained voxels. This, along with the absence of information regarding particle momenta, leads to low signal-to-noise ratios.

4˙1. *Postprocessing image filtering.* – To reduce the noise an asymmetric α-trimmed mean filter [9] has been used. This filter is especially effective if the underlying noise deviates from Gaussian with impulsive components, which is the case for the visible

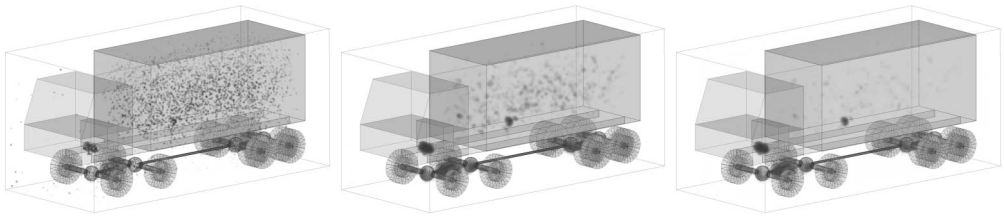

(a) (b) (c)

Fig. 3. – Image reconstruction of a scrap filled truck model containing a 5 liter lead block in a 4 minute acquisition. The image has been processed with a $5 \times 5 \times 5\,\mathrm{cm}^3$ voxel mask and different filters: (a) no filter; (b) Gaussian smoothing; (c) α-trim ($\alpha = 1$).

fluctuations in reconstruction of fig. 3a. Figure 3b represents a simple low-pass filtered image. Figure 3c represents an α-trimmed mean filtered image. For all the algorithms presented, a cubic 125 voxels mask has been used and a Gaussian kernel with σ equal to the voxel size has been applied. The idea of the α-trimmed filter is to look at the neighborhood of every voxels, discarding the upper and lower elements of the mask and to calculate the Gaussian mean value using the rest of them. The noise appears sufficiently dumped whereas the image retains enough information of the hidden source shield.

4˙2. *Momentum estimation.* – A different and complementary strategy would be to reduce the impact of the lack of knowledge of the muon momentum during the image reconstruction process. As already mentioned, the particle momenta are not directly measured in this specific application. The approximation that particles have the same average momentum generates non-Gaussian tails in the s_{ij} distribution of (7) and it contributes to most of the noise and signal fluctuations. A method to estimate each particle momentum has been therefore developed. A particle with a high momentum usually passes almost unperturbed through the tracking detector. As a consequence, the sum of χ^2 of the linear fit in detectors is small. On the other hand, a particle with a low momentum has a higher probability to scatter inside the tracking detector. This results in a higher sum of χ^2. This effect is shown in fig. 4a that represents the scatter plot of the particle momenta *vs.* the χ^2 normalized to the number of tubes crossed. In fig. 4c the effect of the momentum estimation can be compared with the image in fig. 4b that is produced with the perfect knowledge of the simulated momentum.

5. – Results

The efficiency of the presented technique has been tested using a large set of samples for each target. Dataset consisted of 200 reconstructed images of the simulated truck with the container filled with scrap. Half the dataset was hiding a source lead shield (set A) whereas the other half was not (set B). Produced images were analyzed by their density values and a positive state was triggered if a voxel inside the image had a density above a given threshold. The efficiency was computed counting the number of images revealing the actual presence of the lead block (True Positives) and the number of those revealing its actual absence (True Negatives) at a certain density threshold.

To represent the effectiveness of the system we adopted the True Positives and Negatives (TPN) graph [10], which shows the curves of Sensitivity and Specificity overimposed. Measuring the length of the threshold interval in which both curves are close to 100%, it

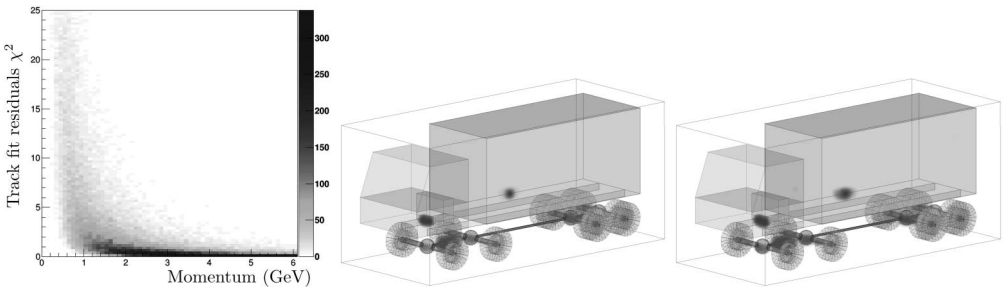

(a) (b) (c)

Fig. 4. – The scatter plot of the particles momenta *vs.* the linear fit χ^2 normalized to the number of tubes crossed (a). Image reconstruction as in fig. 3c: with exact momentum knowledge (b) and using the particle momentum estimation technique (c) see text in sect. **4**˙2.

is possible to highlight a difference in robustness for different configurations. Figure 5a shows the TPN plot when searching for a 5 liter shielding, while fig. 5b shows the TPN plot when searching for a 2 liter shielding, both at two different acquisition times. The TPN representation allows us to identify a threshold in which a known percentage of trucks not triggering an alarm can be dismissed because we are sure a radioactive source shield is not present. All the samples that trigger an alarm at that threshold should be left under examination to gather a higher amount of statistic, in order to enhance the confidence of the identification process. The acquisition time is crucial to improve the performance of the system, as seen in the TPN curves presented, especially when the source shield size is small. These results show that, searching for 5 liter source shields, 60% of controlled trucks can be cleared out in about 2 minutes, while the 100% of them are cleared out in 4 minutes, without missing any of the shields (100% Sensitivity). Searching for 2 liters source shields, about 80% of subjects are cleared out in 4.5 minutes and the 100% in 6 minutes.

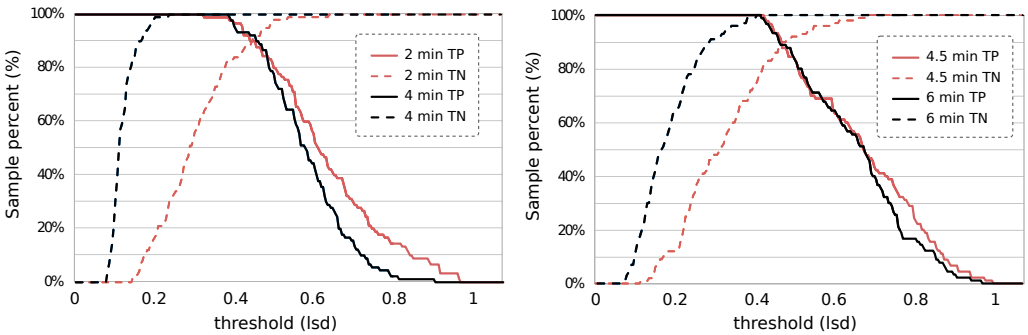

(a) (b)

Fig. 5. – TPN plots testing the efficiency of the system for a 5 liter (a) and 2 liter (b) lead block, built with images from two different acquisition times. Plots represent the sensitivity (solid lines) and the specificity (dashed lines) of the system classifier for different linear scattering density thresholds.

6. – Conclusions

The presented results of the Mu-Steel EU project show the feasibility of detecting shielded radioactive sources using the muon tomography technique. Within the Mu-Steel project a complete portal design has been simulated.

The image filtering algorithm developed represents an improvement of the technique and allows to clean the images from the noise generated by the small statistic that practical applications demand, still preserving a useful signal level. Signal-to-noise ratio has been further enhanced through a particle momentum estimation based on the track fit inside the muon tracking detectors.

We tested the efficiency of the apparatus according to the constraints imposed by industrial standards. The efficiency of this application can reach the 100% of identified source shields in an average time of about 3 minutes for 5 liter and of about 5 minutes for 2 liter shields.

* * *

The MuSteel project was carried out with a grant of the European Commission within the Research Fund for Coal and Steel, RFSR-CT-2010-000033. The research described in the present paper has been made possible by funding from the MuSteel project and the INFN Istituto Nazionale di Fisica Nucleare and the Università degli Studi di Padova (Progetti di Ateneo 2009). I would like to express my deep gratitude to Prof. G. Zumerle and Dr. P. Checchia, supervisors of the project, for their patient guidance and enthusiastic encouragement. Special thanks to my colleagues Dr. M. Furlan and Dr. S. Vanini for their fundamental contributes to this project and their friendship. I wish to acknowledge also all the people in the team of muon tomography from University of Padova, Brescia and Genova in alphabetical order: Dr. L. Barcellan, Dr. M. Benettoni, Dr. G. Bettella, Dr. G. Bonomi, Prof. G. Calvagno, Prof. P. Calvini, Dr. A. Colombo, G. Cortelazzo, Dr. L. Cossutta, Dr. A. Donzella, Dr. F. Gonella, Dr. M. Pegoraro, Prof. S. Squarcia, Dr. M. Subieta, Prof. G. Viesti, Dr. P. Zanuttigh, Prof. A. Zenoni.

REFERENCES

[1] Borozdin K. N. *et al.*, *Nature*, **422** (2003) 277.
[2] Pesente S. *et al.*, *Nucl. Instrum. Methods Phys. Res. A*, **604** (2009) 738.
[3] Research Fund for Coal and Steel research programme of the European Commission, Mu–steel project, *RFSR-CT-2010-000033*, page 547.
[4] Nakamura K. and Particle Data Group, *J. Phys. G*, **37** (2010) 075021.
[5] Yung-Su Tsai, *Rev. Mod. Phys.*, **46** (1974) 815.
[6] Schultz L. J., Blanpied G. S., Borozdin K. N., Fraser A. M., Hengartner N. W., Klimenko A. V., Morris C. L., Oram C. and Sossong M. J., *Image Processing, IEEE Trans.*, **16** (2007) 1985.
[7] Dempster A. P., Laird N. M. and Rubin D. B., *J. R. Stat. Soc. Ser. B*, **39** (1977) 1.
[8] Agostinelli S. *et al.*, *Nucl. Instrum. Methods Phys. Res. Sect. A*, **506** (2003) 250.
[9] Bednar J. and Watt T., *Acoustics, Speech and Signal Processing, IEEE Trans.*, **32** (1984) 145.
[10] Benettoni M., Bettella G., Bonomi G., Calvagno G., Calvini P., Checchia P., Cortelazzo G., Cossutta L., Donzella A., Furlan M., *et al.*, *J. Instrum.*, **8** (2013) P12007.